Electronic Supplementary Material (ESI) for Physical Chemistry Chemical Physics.

Electronic Supplementary Information

Defect chemistry and lithium transport in Li_3OCl anti-perovskite superionic conductor

Ziheng Lu,[a,b] Chi Chen,[a] Zarah Medina Baiyee,[a] Xin Chen,[b] Chunming Niu[b] and Francesco Ciucci[a,]

a. Department of Mechanical and Aerospace Engineering, The Hong Kong University of Science and Technology, Hong Kong, China
b. Center of Nanomaterials for Renewable Energy, State Key Laboratory of Electrical Insulation and Power Equipment, School of Electrical Engineering, Xi'an Jiaotong University, Xi'an 710049, China
c. Department of Chemical and Biomolecular Engineering, The Hong Kong University of Science and Technology, Hong Kong, China

E-mail: francesco.ciucci@ust.hk; Tel: +852 2358 7187

1. The defect structures

Defect structures were computed by initializing the $V_{Li}^{'}$ or the $Li_i^{\bullet}$ at different places (with respect to the counter charge defect) in a 3×3×3 supercell and then minimize the energy using the conjugate gradient algorithm as discussed in Section 2 of the main text. We considered totally three types of charge neutral defect pairs, i.e., the LiCl Schottky pair ($V_{Li}^{'}\text{-}V_{Cl}^{\bullet}$), the Li_2O Schottky pair ($2V_{Li}^{'}\text{-}V_{O}^{\bullet\bullet}$) ,and the Li interstitial with a sustitional O on Cl site. ($Li_i^{\bullet}\text{-}O_{Cl}^{'}$).

For the $V_{Li}^{'}\text{-}V_{Cl}^{\bullet}$ case, there are 6 inequivalent $V_{Li}^{'}$ sites with respect to the $V_{Cl}^{\bullet}$ in a 3×3×3 supercell. So there are 6 different LiCl Schottky structures which are shown in **Fig. S1 (a)**. For the $Li_i^{\bullet}\text{-}O_{Cl}^{'}$ case, when the the $Li_i^{\bullet}$ is initially positioned close to the $O_{Cl}^{'}$, a Li-O dimer forms in the relaxed structure. We found that a small variation of the initial $Li_i^{\bullet}$ position could lead to different orientations of the oxygen-lithium dimer in the end structure. 3 orientations of the Li-O dimer were obtained in our calculations and they are shown in **Fig. S1 (b)**. When the $Li_i^{\bullet}\text{-}O_{Cl}^{'}$ are separated, the interstitial Li inserts into the lattice by forming a Li-Li dumbbell. Due to the possible combinations of Li-Li dumbbell orientations and Li-Li dumbbell positions (with respect to the $O_{Cl}^{'}$), the number of $Li_i^{\bullet}\text{-}O_{Cl}^{'}$ structures is large. In **Fig. S1 (b)**, we show the ones we computed. For the $2V_{Li}^{'}\text{-}V_{O}^{\bullet\bullet}$ case, although there are also large number of possible structures due to the combination of $V_{Li}^{'}$ sites, we only calculated 4 structures and they are shown in the main text (**Fig. 3**)

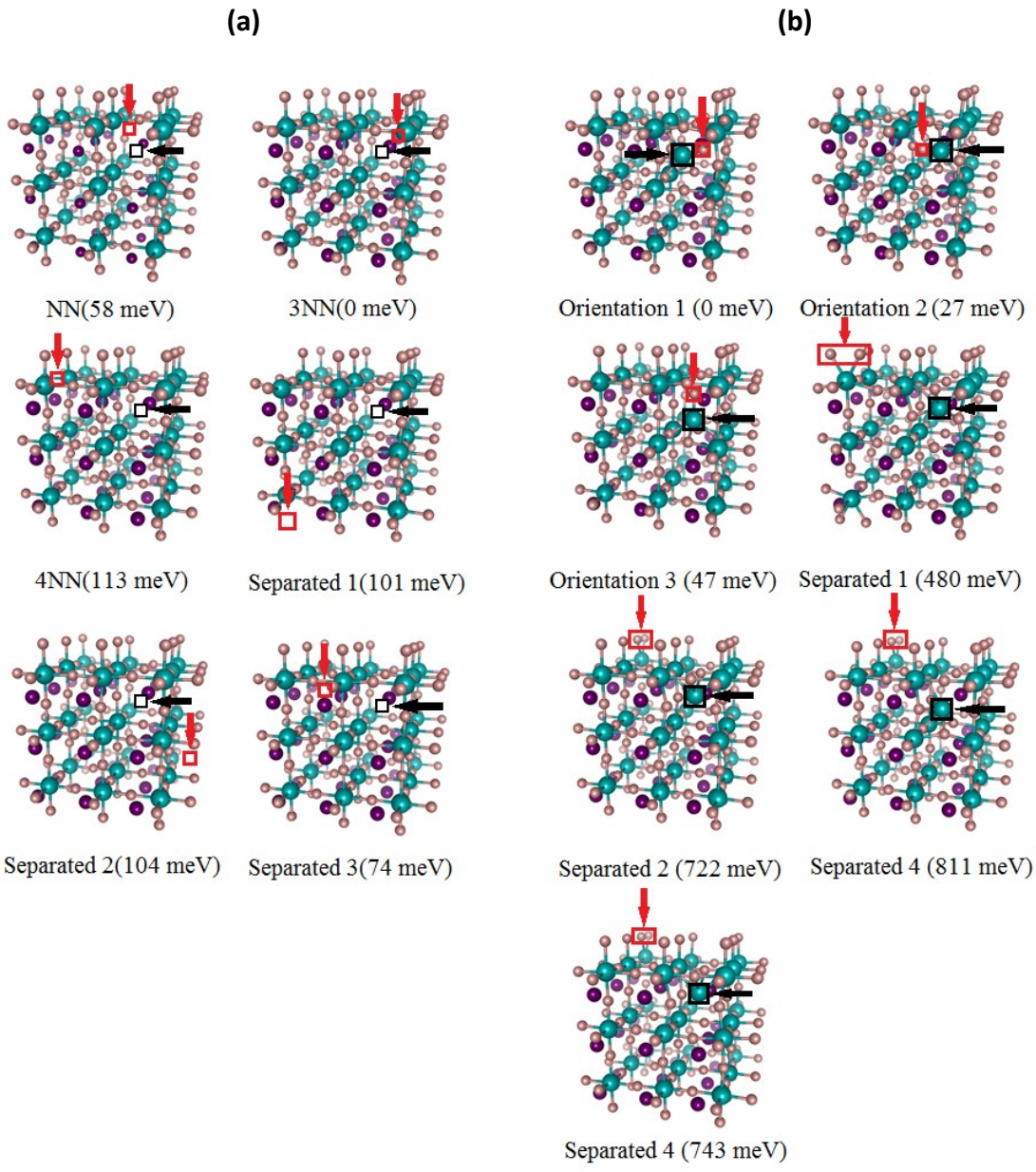

Fig.S1 The computed defect structures of (a) the LiCl Schottky pair (V'_{Li}-$V^{\bullet}_{Cl}$) and (b) the Li interstitial with a substitutional O on the Cl site ($Li^{\bullet}_{i}$-O'_{Cl}). Arrows and hollow squares are used to highlight the $V^{\bullet}_{Cl}$ (black) and the V'_{Li}(red) in (a) (O'_{Cl} (black) and the $Li^{\bullet}_{i}$(red) in (b)).

2. The calculation of defect binding energies

We calculated the defect binding energies to quantitatively study the defect interactions. The calculation of binding energy is conducted using a supercell approach following the work by M. Nakayama *et al.* [1]

$$E_{binding} = \sum E_{isolated} - (E_{perfect} + E_{pair})$$

where $E_{binding}$, $E_{isolated}$, $E_{perfect}$, and E_{pair} are the binding energy of a defect pair, the energy of a perfect supercell, the energy of a supercell containing the defect pair and the energy a supercell containing the individual defect, respectively. To be more specific, the binding energy of V'_{Li}-$V^{\bullet}_{Cl}$ in the main text is calculated using a 3×3×3 supercell by

$$E_{bindV_{Li}-V_{Cl}} = \left(E(Li_{81}O_{27}Cl_{26}, +|e|) + E(Li_{80}O_{27}Cl_{27}, -|e|)\right) - \left(E(Li_{81}O_{27}Cl_{27}) + E(Li_{80}O_{27}Cl_{26})\right)$$

where $E_{bindV_{Li}-V_{Cl}}$, $E(Li_{81}O_{27}Cl_{27})$, $E(Li_{80}O_{27}Cl_{26})$, $E(Li_{81}O_{27}Cl_{26}, +|e|)$, $E(Li_{80}O_{27}Cl_{27}, -|e|)$ are the binding energy of a V'_{Li}-$V^{\bullet}_{Cl}$ pair, the energy of a 3×3×3 supercell with one V'_{Li}, the energy of a 3×3×3 supercell with one $V^{\bullet}_{Cl}$, the energy of a 3×3×3 supercell with no defects and the energy of a 3×3×3 supercell with a V'_{Li}-$V^{\bullet}_{Cl}$ pair. For all energy calculations, we used the lowest energy structure as discussed in previous section and assumed the same chemical potential of the electron reservoirs when considering the charged individual defects. [1]

3. The low energy migration pathways

For the computation of the low energy lithium migration pathways, we used 3×3×3 supercells containing one $V_{Li}^{'}$-$V_{Cl}^{\bullet}$ pair ($Li_{80}O_{27}Cl_{26}$). By taking advantage of the periodic boundary conditions we were able to consider three different separations between $V_{Cl}^{\bullet}$'s (11.7 Å, 16.4 Å and 20.2 Å). For each separation, we picked only pathway out of all the possibilities. The calculation of a specific pathway was done by manually choosing $V_{Li}^{'}$ sites as intermediate steps (intermediate structures). For example, in **Fig S2 (a)**, the intermediate structures are NN, 3NN, 4NN, 3NN and NN, which means one Li ion on 3NN will first jump to NN site, then another Li ion on 4NN site will jump to 3NN site, etc. Energy barrier of each jump was then calculated based on DFT-NEB using 5 images. **Fig S2** shows the three calculated Li migration pathways. TS_x_y (x and y are the name of the intermediate structures) is used to represent the transitional states between the intermediate structures x and y. Red squares are used to highlight the $V_{Li}^{'}$ positions during the migration process.

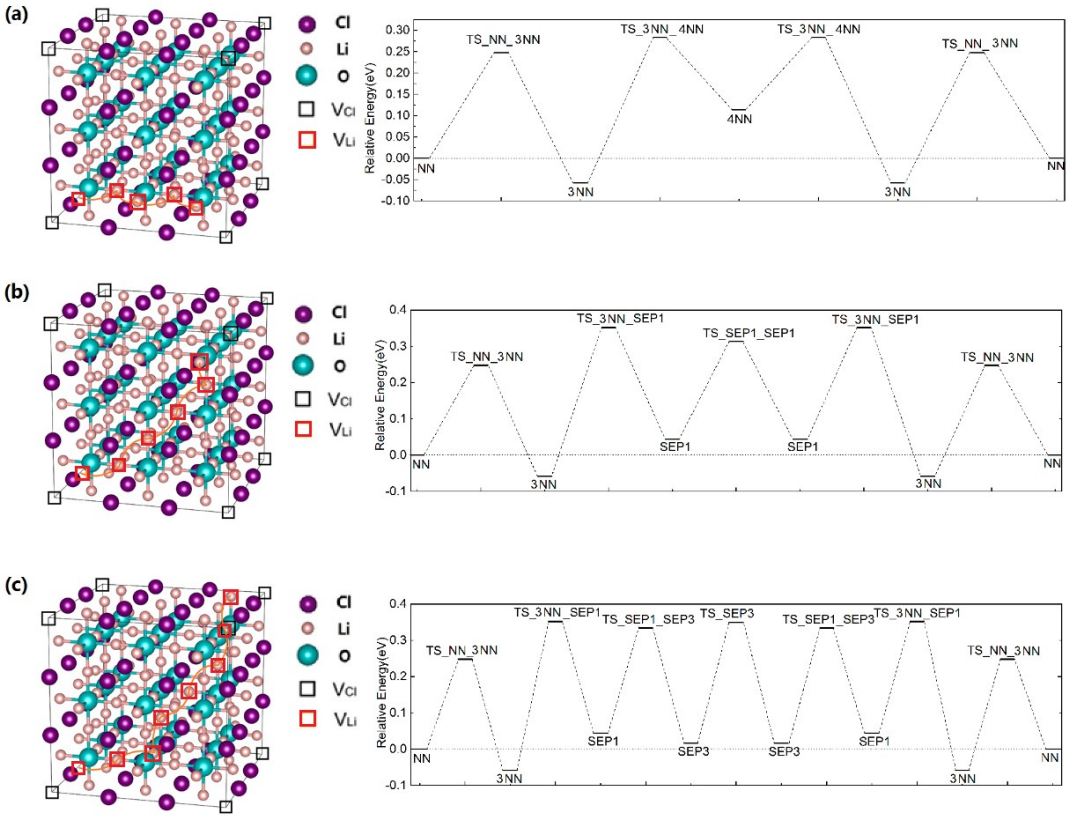

Fig.S2 The migration pathways between two $V_{Cl}^{\bullet}$'s separated by a distance of (a) 11.7 Å, (b) 16.5 Å and (c) 20.2 Å and the corresponding energies. The NN (Nearest Neighbor), 3NN (the third Nearest Neighbor), 4NN (the forth Nearest Neighbor), SEPx (Separated x) clarify where the Li vacancies are. They correspond to the structures shown in **Fig. S1**. TS states are used to represent the transitional states between global or local minima. Red squares are used to highlight the $V_{Li}^{'}$ positions during the migration process.

4. Typical MSD curves

Mean squared displacements were computed in order to determine the Li ion diffusion coefficients as described in Section 2 in the main text. **Fig.S3** presents typical MSDs of Li in defect-free, Li deficient and Li excess systems. In agreement with reported results, the displacements of Li ions in defect-free systems do not grow with time which means Li ions are vibrating around their stable positions with no effective jump.[3] The slope of MSDs in the LiCl deficient systems are bigger than that of the Li excess and the Li_2O deficient systems corresponding to a higher mobility of Li ions in LiCl deficient systems than the other two. Another difference between the three sets of MSD curves as shown in **Fig.S3** is the smoothness. The rougher curves for the $Li_{2.950}O_{0.925}Cl$ and the $Li_{3.050}O_{2.950}Cl_{2.950}$ systems compared with the $Li_{2.950}OCl_{0.950}$ systems indicate a longer time for the charge carrier to make an efficient jump.

(a)

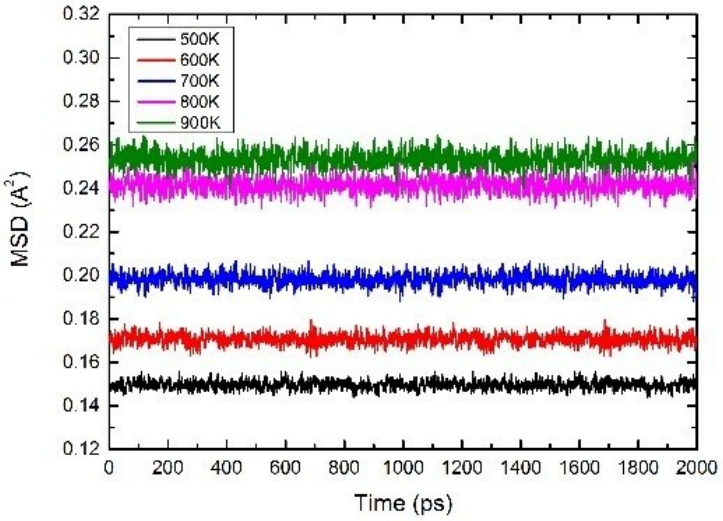

(b)

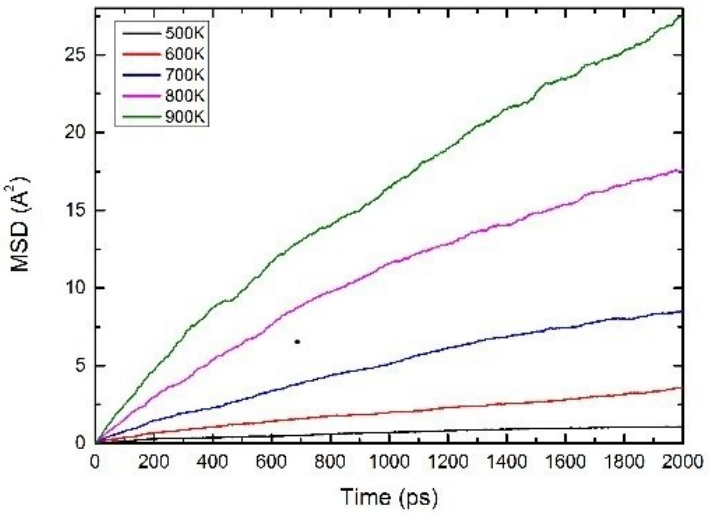
500K
600K
700K
800K
900K
MSD (Å²)
Time (ps)
0
5
10
15
20
25
0
200
400
600
800
1000
1200
1400
1600
1800
2000

(c)

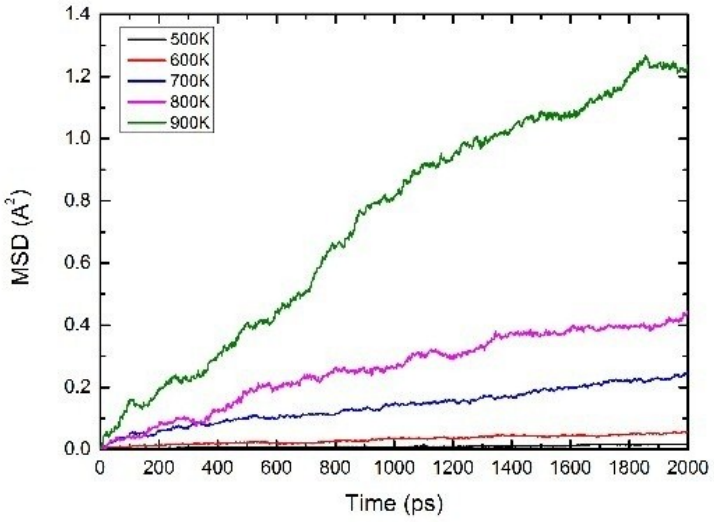
500K
600K
700K
800K
900K
MSD (Å²)
Time (ps)
0.0
0.2
0.4
0.6
0.8
1.0
1.2
1.4
0
200
400
600
800
1000
1200
1400
1600
1800
2000

(d)

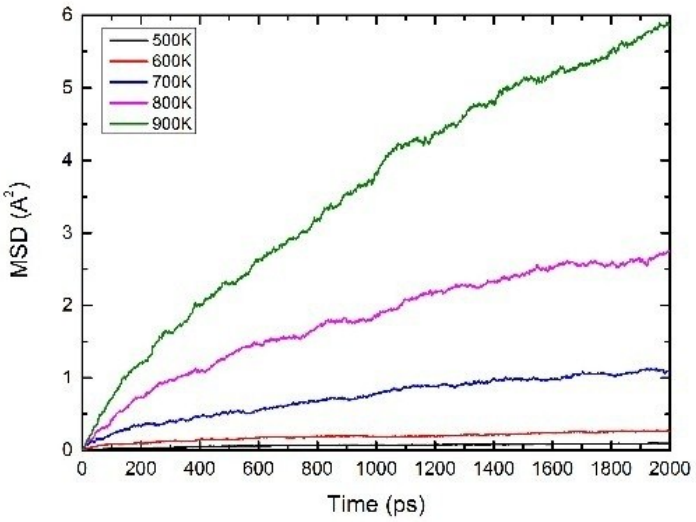

Fig.S3 Typical mean squared displacements of lithium ions in (a) Li_3OCl (b) $Li_{2.950}OCl_{0.950}$ (c) $Li_{2.950}O_{0.925}Cl$ and (d) $Li_{3.050}O_{2.950}Cl_{2.950}$

References

1. M. Nakayama and M. Martin, *Phys. Chem. Chem. Phys.*, 2009, **11**, 3241-3249.
2. Y. Zhang, Y. Zhao and C. Chen, *Phys. Rev. B:*, 2013, **87**, 134303.